Proteomics of Patient-derived Breast Tumours Identifies a Pro-migratory Osteomodulin-Cyclin Dependent Kinase 1 Axis which Drives Bone Metastasis

Joseph Parsons[1,2], Hannah Harrison[1,7], Thomas Kedward[2,7], Paul Fullwood[2], Sara Cabral[1,7], Katherine Spence[1,7], Danielle Barden[2], Jennifer Ferguson[2], Joanne Watson[2], Kalliopi Tsafou[3], Caron Behan[4], Nisha Ali[5,7], Michael P. Smith[2], Ciara O'Brien[1,6,7,*], Robert B. Clarke[1,7,*], Chiara Francavilla[2,7,8, *, #]

[1]Division of Cancer Sciences, School of Medical Sciences, Faculty of Biology Medicine and Health, University of Manchester, Manchester UK

[2]Division of Cellular and Molecular Function, School of Biological Sciences, Faculty of Biology Medicine and Health, University of Manchester, Manchester UK

[3] The Broad Institute of MIT and Harvard, Cambridge, MA.

[4]Histology Cancer Research UK Manchester Institute, Manchester UK

[5]Manchester University Foundation Trust, Wythenshawe Hospital, Manchester UK

[6]Department of Medical Oncology, Christie Hospital, Manchester UK

[7]Manchester Breast Centre, University of Manchester, Manchester UK

[8]DTU Bioengineering, Danish Technical University, Lyndby, Denmark

*Co-senior authors

#Corresponding Author:

Chiara Francavilla

Oxford Road

Manchester

M13 9PT

Tel: +44 161 275 5208

Emails: chiara.francavilla@manchester.ac.uk and chiafra@dtu.dk

Keywords: breast cancer, bone metastasis, proteomics, phosphoproteomics, precision medicine, osteomodulin, CDK1, MDAMB231

Number of Figures: 6

Number of Tables: 0

Number of Supplemental Figures: 6

Number of Additional Files: 15

Word counts: 5032

Abstract

Breast cancer remains a leading cause of mortality, predominantly due to the development of metastases to vital organs. At present, predictive biomarkers of organ specific metastasis and therapies targeted to the metastatic niche are limited. Here, to identify the molecular determinants of breast cancer metastasis we analysed patient-derived breast tumours by combining quantitative proteomics, bioinformatics, and functional assays *in vitro* and *in vivo.* We identified elevated levels of the protein Osteomodulin (OMD) associated with breast cancer bone metastases in patient-derived samples. OMD overexpression in the breast cancer MDA-MB-231 cell model significantly increases cell migration *in vitro* and promotes the formation of bone metastases *in vivo*. Phosphoproteomics analysis of MDA-MB-231 cells expressing OMD identifies active Cyclin-dependent kinase 1 (CDK1) downstream of OMD. The importance of the OMD-CDK1 axis was validated using two independent phosphoproteomics datasets analysing patient-derived breast cancer samples. We also show that the OMD-CDK1 axis drives cell migration and cell viability *in vitro* and the formation of bone metastases *in vivo*. Finally, CDK1 inhibition reduces *in vitro* cell viability of

an independent cohort of metastatic patient samples showing high CDK1 activity. Therefore, the OMD-CDK1 axis will determine which breast cancer patients develop bone metastases and is a therapeutic target to treat or prevent breast cancer bone metastases.

Introduction

Metastases are responsible for 90% of breast cancer deaths (1) and are most commonly found in the bone, brain, liver and lungs of breast cancer patients (2). Although different drivers depending on the metastatic organ have been identified (3), there are currently neither clinically available biomarkers nor targeted drug therapies against organ-specific metastases in breast cancer. For instance, preventing bone metastasis or targeting of bone organotropic drivers would greatly benefit patients given the capacity of the bone microenvironment to condition tumour cells to colonise other organs (4). Currently, radiologically detected, or symptomatic bone metastases are managed with bisphosphonates and Receptor Activator of NFκB Ligand (RANKL) inhibitors (4). However, there is still the need to discover more specific biomarkers and actionable combinations of therapeutic targets for patients who may develop metastasis to the bone and other organs.

Omics technologies have nowadays the capacity to provide novel biomarkers and therapeutic targets from a variety of samples, including patient-derived samples (5). For instance, genomic analysis of metastatic breast cancer patient samples or matched primary and metastatic breast cancer patient samples identified several potential therapeutic targets whose mutation was enriched in metastases (6). Also transcriptomic analysis of breast cancer primary and metastatic samples identified several transcripts dysregulated in breast cancer bone metastases compared to other metastatic sites (7). In contrast to genomics and transcriptomics, proteomics and phosphoproteomics have so far analysed primary breast cancer but not metastatic samples (8), for example identifying dysregulation in tumour cells metabolism (9), novel kinases in triple negative breast cancer patients (10), and signalling

pathways associated with Epidermal Growth Factor Receptor 2 (HER2)-targeted therapy resistance (11).

Here, to identify potential therapeutic targets and their biomarkers in breast cancer metastasis organotropism we analysed fresh frozen primary breast cancer resection samples that were clinically annotated as to the presence or absence of organ-specific metastases within 5 years of diagnosis. We combined mass spectrometry-based proteomics and phosphoproteomics, bioinformatics, and functional assays *in vitro* and *in vivo*. We identified the Osteomodulin (OMD)-Cyclin Dependent Kinase (CDK1) axis to be dysregulated in primary breast cancer samples associated with bone metastasis and validated the pro-migratory and pro-metastatic role of the OMD/CDK1 axis in breast cancer models and independent cohorts of patient-derived samples. Thus, our omics approach identifies a novel mechanism promoting breast cancer bone metastases.

Material and methods

Reagents

A detailed list can be found in Additional File 1.

Cell Culture

All cells were authenticated using short tandem repeat analysis of 21 markers by Eurofins Genomics and Cancer Research UK Manchester Institute Molecular Biology Core Facility in 2021 and 2022. Cells were tested monthly for mycoplasma with a PCR-based detection assay (VenorGeM-Cambio). MDA-MB-231 breast cancer cells were a gift from J. Massague (12). HMFU19 and 544R Cancer-Associated Fibroblasts (CAFs) (13, 14) were a gift from C. Kirwan, University of Manchester. HFOB 1.19 were purchased from ATCC (CRL-11372). RAW264.7 cells (15) were a gift from P. Ottewell, University of Sheffield. MDA-MB-231, 544R CAFs, Lenti X cells (gift from A. Hurlstone, University of Manchester), and RAW 264.7 cells were grown in DMEM supplemented with 10% Fetal Calf Serum (FCS), 1% Penicillin-Streptomycin (Pen-Strep) (100U/ml penicillin, 100ug/ml streptomycin) and 1mM Sodium

Pyruvate. HFOB 1.19 cells were grown in DMEM-F12 supplemented with 10% FCS and 1% Pen-Strep. HMFU19 cells were grown in RPMI supplemented with 10% FCS, 1% Pen-Strep and 2mM L-Glutamine. RAW264.7 cells were differentiated by treatment with 100ng/ml recombinant human RANKL for 8 days (16). HFOB 1.19 cells were differentiated by 7 days of culture at 39.5^{o}C with undifferentiated cells being grown at 34°C (17). All cells were grown in humidified 5% CO_2 incubators. To create MDA MB 231 cells or MDA MB 231 bone variant cells expressing osteomodulin (PAO, BOO) or the mApple control (PAM, BOM), a pCDH1-Ef1-MCS-T2A-mApple vector (18) was used. The pCDH1 vector and either the mApple amplified gene with a stop codon or an osteomodulin encoding gene string (ThermoFisher) were cleaved with NotI and NheI restriction enzymes and then ligated using a T4 ligase overnight. LentiXL cells at 70% confluency were transfected with Fugene, plasmid and viral packaging proteins pMDL, VSVG and Rev following standard protocols. Lentivirally transfected cells were sorted using fluorescence activated cell sorting (BD FACSAria III Fusion Cell Sorter) to have similar expression of mApple.

Sample Preparation and Analysis for Mass Spectrometry-based Proteomics and Phosphoproteomics and Data Analysis

A detailed protocol can be found in the Supplementary Materials and Methods (18).

In vivo Experiments

All *in vivo* experiments were performed in accordance with the UK Home Office Animals (Scientific Procedures) Act 1986 under project license PCFEAC0D4 and study protocols were approved by the CRUK Manchester Institute Animal Welfare and Ethical Research Board (AWERB). 100,000 PAM, PAO, or BOM cells in 50µl PBS were injected into the left cardiac ventricle of 4 athymic nude mice (sourced from Envigo) per condition using a 28-gauge needle. Mice were monitored for 25 days before culling. For CDK1 inhibition studies, 4 days after intracardiac injection of 100,000 PAO cells, 4 athymic nude mice were dosed with 225ul of RO-3306 solution (final concentration 4mg/kg, SeleckChem) dissolved in 40%

PEG300-1% Tween80-3% DMSO in ddH_2O given 3 times per week by oral gavage and compared to 4 vehicle control mice. Mice were culled 25 days after intracardiac injection of breast cancer cells. Lungs (only for the first study) and one femur were formalin-fixed for immunohistochemical analysis, and one femur was collected in DMEM with FCS, 10% Pen-Strep and 1mM Sodium pyruvate and bones were flushed. To flush bones, the ends of mouse femurs were clipped using scissors and ground down and the bone marrow was flushed using 5mL complete DMEM using a 25-gauge needle. The ground bone ends and bone marrow were filtered through a 100µm filter which was washed with 5mL complete DMEM. Filtered bone cells were pelleted by centrifugation at 600xg at $4^{o}C$ before filtering through a 40µm filter.

Immunohistochemistry

A detailed protocol can be found in Additional File 1.

Biochemical Assays

Detailed protocols for quantitative RT-PCR, cell lysis and immunoblotting, EdU incorporation assay, collagen contractility assay, Boyden chamber invasion assay, scratch wound cell migration assay, mammosphere assays, alkaline phosphatase activity assay, alizarin red staining, bone resorption assay, Alamar blue cell viability assay can be found in Additional File 1.

Statistics

Experiments were performed in at least three independent biological triplicates. One-way ANOVAs with Dunnett's multiple comparisons test were used to determine significance between 3 or more experimental conditions. Student's t tests were used to determine significance between two experimental conditions.

Results

Proteomic Analysis of Primary Breast Cancer Samples Identifies Dysregulation of Osteomodulin (OMD) in Patients Developing Bone Metastases

To identify changes in proteins and phosphorylated proteins underlying breast cancer metastasis, we analysed a cohort of 39 primary breast cancer patient samples, of which 21 developed metastases within 5 years of diagnosis (metastatic) while 18 did not (non-metastatic), by label-free mass spectrometry-based proteomics and phosphoproteomics (Fig. 1A, Additional Files 2-4). Of the 39 patient samples, 21 were from patients who had hormone receptor positive (HR+) tumours, 9 who had human epidermal growth factor receptor 2 positive (HER2+) tumours and 9 who had triple negative (TN) tumours. Our patient cohort included patients who developed metastases at all four of the main metastatic sites in breast cancer at 5 years post-diagnosis (bone, brain, liver and lung) (2), thus providing a unique dataset (Fig. 1A, Additional File 2). We identified and quantified a total of 6293 proteins (5106 in non-metastatic samples and 5741 in metastatic samples) and 14281 phosphorylated sites (11148 in non-metastatic samples and 13186 in metastatic samples) (Supplemental Fig. 1A-B, Additional Files 3-4). Pearson correlation for technical replicates in the proteomics data was above 0.95 on average and was above 0.6 on average in the phosphoproteomics data (Supplemental Fig. 1C-D), thus showing high correlation. Across phosphorylated sites, 62.8% were singly phosphorylated, 29.0% were doubly phosphorylated and 7.2% were more than doubly phosphorylated and the residue distribution across serine, threonine and tyrosine was 88.24%, 10.92%, 0.83%, respectively with a median score for phosphorylated peptides of 172 (Supplemental Fig. 1E-G). Therefore, the quality of our proteomics and phosphoproteomics analysis was consistent with previous publications (8, 18).

We focused on proteins and phosphorylated sites present in at least 80% of either non-metastatic or metastatic samples for further analysis (Additional Files 5-6). Differential expression analysis of patients who developed or did not develop metastases identified 33 differentially regulated proteins and 156 differentially regulated phosphorylated sites on 122

proteins (p value <0.05, Log2 Fold Change in intensity >1.5) (Fig. 1B-C, Additional Files 5-6). To determine whether these differentially regulated proteins and phosphorylated sites had previously been associated with breast cancer metastasis, we compared our list of 33 dysregulated proteins and 156 dysregulated phosphorylated sites with an in-house curated database of metastasis-associated genes and proteins obtained by searching PubMed with the term “Breast Cancer Metastasis” for a total of 2472 entries (Additional File 7). We found that ADIRF, CMA1, COL11A1, COL4A1, CTHRC1, MXRA5, OGN, OMD, SNCG, SYNM, TNC proteins and BAD, MAPK1 (2 sites), PGRMC1 (2 sites), STMN1, EIF4B and VIM phosphorylated sites have been previously associated with breast cancer metastasis or metastasis-promoting phenotypes (Fig. 1B-C, Additional Files 5-7). Thus, our proteomics and phosphoproteomics analysis identified both known and novel drivers of breast cancer metastasis.

Next, KEGG and GO biological processes enrichment analysis identified several processes enriched among the upregulated proteins and phosphoproteins, including collagen remodelling, previously associated with breast cancer (19) (Fig. 1D, Additional File 8). Among the upregulated proteins and phosphorylated sites associated with collagen synthesis and remodelling, the member of the small leucine-rich repeat protein family Osteomodulin (OMD) (20) was the only one previously associated with bone tropism (7). Indeed, we found that OMD expression was significantly higher in patients who developed bone metastasis compared to patients who developed metastases in other sites (p value = 0.0012), or that did not develop metastases (p value = <0.0001) (Fig. 1E, Additional Files 2, 4). Consistent with the idea that OMD expression is associated with bone metastasis, we found that the expression of OMD mRNA was also significantly higher in bone metastases compared to other metastatic sites in independent breast (FDR adjusted p value = 0.00000364) (Fig. 1F) and prostate cancer GEO datasets (7, 21).

Overall, our proteomics analysis of primary breast cancer samples suggests that OMD expression is associated with breast cancer bone metastasis.

OMD Does Not Alter the Behaviour of Fibroblasts, Osteoblasts, or Osteoclasts Cell Models

To study how OMD may contribute towards bone metastasis, we assessed the localisation of OMD by immunohistochemistry on 25 of the 39 patient samples for which formalin-fixed paraffin-embedded (FFPE) sections were available (Additional File 2). We found that 17 samples stained positive for OMD showing heterogeneous OMD expression in the tumour, stromal and immune compartments (Supplemental Fig. 2). However, haemotoxylin and eosin (H&E) staining on these 25 sections evaluated by a pathologist showed that 20 out of 25 samples had >50% epithelial content with an overall average epithelial content of 66% (Additional File 2), indicating that our omics analyses were largely based on epithelial cancer cells. Based on these findings, we next tested whether OMD affected bone metastases through cells in the microenvironment or through the epithelial tumour cells themselves.

To verify this hypothesis, we used available cell models of the primary and secondary (bone) tumour microenvironment including normal and cancer-associated fibroblasts (HMFU19 and 544R, respectively) (13, 14), osteoblasts (HFOB 1.19) (17), and osteoclasts (RAW 264.7, post-differentiation with RANKL) (15). As a model of tumour epithelial cells, we used the epithelial breast cancer cell line MDA-MB-231 infected with lentivirus expressing either mApple as a control (PAM) or an OMD-T2A linker-mApple construct (PAO) (Fig. 2A-B). OMD expression was confirmed by immunoblotting in cell lysates from both starvation and complete media and in conditioned medium (Fig. 2A-B), thus confirming that OMD is a secreted protein (20). To study how OMD may affect the cells of the breast microenvironment, we tested whether OMD affects matrix remodelling, given the known role of OMD in collagen remodelling (22) and of fibroblasts and osteoblasts in remodelling the extracellular matrix in primary tumours (23). To mimic matrix remodelling we used a collagen contractility assay (24). We assessed the effect of conditioned medium from PAO (containing OMD) compared to conditioned medium from PAM as a control on the ability for collagen contractility of HMFU19, 544R, and differentiated HFOB 1.19 cells (Fig. 2C-E). To

mimic secreted OMD, we used recombinant OMD (rOMD) at increasing concentrations from 10ng/ml to 1µg/ml (22). Neither conditioned media nor rOMD significantly affected the collagen remodelling capabilities of any tested cells (Fig. 2C-E). We next tested osteogenesis, a key process in differentiation and turnover of bone tissues involved in sclerotic metastases (25), by alkaline phosphatase assay (26) and calcium deposition, crucial for osteosclerotic bone metastases (25), via Alizarin red assay (27). Both osteogenesis and calcium deposition were significantly induced in the HFOB 1.19 osteoblast cell models upon differentiation when grown at 39.5^{o}C (Fig. 2F-G, Supplemental Fig. 3A). However, compared to differentiated HFOB 1.19 osteoblasts, neither alkaline phosphatase activity nor Alizarin red assay by differentiated HFOB 1.19 were significantly altered by conditioned medium from PAM or PAO or by increasing concentrations of rOMD, except for the highest concentration of rOMD affecting only calcium deposition (Fig. 2F-G, Supplemental Fig. 3A). Finally, we assessed the activity of osteoclasts, another key cell type for breast cancer bone metastases (25), by determining the ability of an osteoclast cell model (RAW 264.7 mouse monocytes) to create pores in the bone matrix, a process known as bone resorption (25). RAW 264.7 cells were differentiated to osteoclasts using RANKL treatment (16) and differentiation was assessed by quantitative RT-PCR expression of OSCAR and CTSK genes, which are both markers of osteoclast differentiation (15) (Supplemental Fig. 3B). No significant induction of osteoclast activity was seen upon treatment of differentiated RAW 264.7 cells with either conditioned media from PAM or PAO cells or rOMD was observed, as the number and size of pores was consistent across all conditions (Fig. 2H-I, Supplemental Fig. 3C).

Taken together, these findings suggest that secreted OMD does not promote extracellular matrix remodelling, only partially affects osteoblast activity, and does not play a role in bone resorption and osteoclast activity in the tested experimental models of tumour microenvironment.

OMD Increases Breast Cancer Cell Migration *in vitro* and Bone Metastasis *in vivo*

To address whether OMD expression affected the behaviour of epithelial breast cancer cells we tested whether OMD expression affected extracellular matrix remodelling by a collagen contractility assay and found that collagen remodelling was not affected by OMD expression in our PAM vs PAO cell model (Fig. 2A-B, Supplemental Fig. 4A). Next, we assessed whether OMD altered cell proliferation by measuring EdU incorporation and found no significant effect of OMD expression on proliferation (Supplemental Fig. 4B). As OMD has previously been associated with resistance to apoptosis (28), we also tested whether OMD expression affected anoikis resistance and stemness of breast cancer cells through mammosphere formation and mammosphere self-renewal assays. OMD expression showed no significant effect on mammosphere formation or self-renewal (Supplemental Fig. 4C-D). Finally, to assess the effects of OMD on cell motility through matrix we measured cell invasion by a Boyden chamber assay with Matrigel-coated chambers and cell migration via a scratch wound assay where proliferation was prevented by mitomycin pre-treatment (29). Although invasion was not significantly altered between PAM and PAO cells in our experimental conditions, OMD expression significantly increased cell migration (Fig. 3A-B, Supplemental Fig. 4E). Also increasing concentrations of rOMD significantly increased PAM cell migration (Fig. 3A-B). However, OMD expression did not affect cell motility of the bone-tropic MDA-MB-231 cell line (12) (Fig. 3C-Supplemental Fig. 4F-G). Altogether, these findings suggest that OMD has mainly a pro-migratory role in our model of breast cancer epithelial cells.

Given the increased migratory capacity of PAO compared to PAM *in vitro* and on the increased expression of OMD in patients who developed bone metastases compared to patients who did not develop metastases or developed metastases in other organs (Fig. 1E and 3A-B, Additional Files 3-5), we next assessed the metastatic potential of PAO and PAM cells *in vivo*. We injected PAM, PAO, and BOM (positive control for bone metastases) cells by intracardiac injection into four athymic nude mice and firstly counted the number of lung metastatic lesions as a measure of their metastatic potential. We found no significant

differences in the metastatic potential of PAM, PAO, and BOM cells (Fig. 3E). However, the number of cytokeratin 19 (CK19)-positive cells in bone flushes, which is an indicator of the number of human epithelial cells in mouse bones (12), was significantly higher in both BOM and PAO compared to PAM cells (Fig. 3F-G). This finding not only confirms the bone tropism of BOM cells (12), but also supports a role for OMD in colonising the bones *in vivo*.

Overall, this data suggests that the pro-migratory function of OMD in breast cancer epithelial cells may prime primary breast cancers for bone metastasis.

Phosphoproteomics Identifies an OMD-CDK1 axis Driving Cell Migration and Viability *in vitro* and *in vivo*

To determine the mechanism underlying OMD-dependent cell migration *in vitro* and bone colonisation *in vivo*, we analysed changes in the proteome and phosphoproteome of PAO cells compared to PAM, BOM, and BOO cells as controls (Supplemental Fig. 5A). We identified and quantified 3971 proteins and 9423 phosphorylated sites (Additional Files 9-10). Pearson correlation between biological replicates of the proteomic and phosphoproteomics data were consistently over 0.97 and 0.6 respectively (Supplemental Fig. 5B-C). Across phosphorylated peptides, 41.9% were singly phosphorylated, 47.6% were doubly phosphorylated, and 10.5% were more than doubly phosphorylated and the distribution of phosphorylated site residue across serine, threonine and tyrosine was 85%, 11.3% and 3.7%, respectively indicating enrichment on tyrosine residues, with a median phosphorylated peptide score of 182 (Supplemental Fig. 5D-F). All the quality controls were in line with previous publications (8, 18). Differential expression analysis (P value <0.05, Log2 Fold change >1) of these high-quality datasets did not identify significantly differentially regulated proteins between PAO and PAM cells (Additional File 11) but did identify 53 differentially regulated phosphorylated sites, of which 18 were upregulated and 35 were downregulated (Fig. 4A, Additional File 12). Of the 18 phosphorylated sites specifically upregulated in PAO compared to PAM, only FOS like 1 (FOSL1) phosphorylated on serine

26 has a known cancer-associated function according to Phosphosite plus (30) and has been shown to promote migration in MCF7breast cancer cells (31). Of the 35 downregulated phosphorylated sites in PAO compared to PAM, 5 were also downregulated in BOO compared to BOM, suggesting that these sites are unlikely associated with the PAO pro-migratory signalling mechanism and thus they were excluded from further analysis (Additional File 12). Of the remaining 30 phosphorylated sites specifically downregulated in PAO compared to PAM cells, six had metastasis-associated functions, such as promoting cell migration, invasion, or drug resistance according to Phosphosite plus (30) (Fig. 4A). Only one of these 30 downregulated sites was associated with inactivation of protein activity: Tyrosine 15 on the cell cycle regulator, Cyclin-dependent kinase 1 (CDK1, CDC2) (32) (Fig. 4A, Additional File 12). We confirmed the downregulation of Y15 on CDK1 in PAO compared to PAM, BOO and BOM cells by quantified immunoblotting (Fig. 4B-C). Interestingly, we found an inverse relationship between OMD expression and reduction of CDK1 inhibitory phosphorylation in two independent phosphoproteomics datasets analysing breast cancer patients (105 and 122 patients, respectively) (8, 33). These phosphoproteomics analyses showed that CDK1 inhibitory phosphorylation at T14, Y15, and Y19 (32) was significantly reduced in patients where OMD expression was above the mean compared to patients where OMD expression was below the mean (Fig. 4D-E). Therefore, the OMD-CDK1 axis may regulate the OMD-dependent phenotypes *in vitro* and *in vivo*.

To verify the role of CDK1 in cell migration we inhibited CDK1 using 10µM of the CDK1 inhibitor (CDK1i) RO-3306 (34) and assessed cell migration in the PAM and PAO model system. Besides confirming that PAO cells migrate more than PAM cells, we found that PAO but not PAM cell migration was significantly reduced upon treatment with 10µM RO-3306 (Fig. 5A). To test whether this reduction in migration was specifically downstream of CDK1, we inhibited CDK4 and CDK6 with 10µM of the clinically relevant inhibitor Palbociclib (CDK4,5i) and showed that CDK4/6 inhibition did not significantly reduce PAO cell migration (Fig. 5B). Therefore, CDK1, but not CDK4-6, is specifically activated in PAO cells to regulate

cell migration *in vitro*. To test whether CDK1 inhibition also affected cell viability we performed an Alamar blue assay (35) on the PAM and PAO cell model system. We found that CDK1 inhibition significantly reduced the viability of PAO, but not PAM cells (Fig. 5C), suggesting that enhanced CDK1 activity is required for sensitivity to CDK1 inhibition.

Since CDK1 regulate cell migration and viability in PAO cells, we next tested whether the OMD-CDK1 axis regulated bone colonization *in vivo.* To do this, we performed intracardiac injection of PAO cells into four athymic nude mice and tested whether inhibition of CDK1 affected the formation of bone metastasis. We detected numerous cytokeratin 19 (CK19)-positive cells in bone flushes of mice treated with the vehicle control but almost no CK19-positive cells in those treated with the CDK1 inhibitor RO-3306 (Fig. 5D-E). Therefore, this data suggests a role for the OMD-CDK1 axis in colonising the bones *in vivo.*

Finally, we tested the clinical relevance of these findings using patient-derived breast cancer cells acquired from metastatic pleural effusions and ascitic fluids (Additional File 13). We assessed the effect of CDK1 activity on the viability of five metastatic patient-derived breast cancers *in vitro*. We found that 4 of the 5 metastatic tumour samples had decreased cell viability in response to CDK1 inhibition using the Alamar blue assay (Fig. 5F). Phosphoproteomics and proteomics analysis of these samples produced a high-quality dataset (Supplemental Fig. S6, Additional Files 14-15). Although we did not detect OMD in the proteome dataset (Additional File 14), we identified downregulation of Y15 on CDK1 in the four samples that responded to CDK1 inhibition (Fig. 5G, Additional File 15). Thus, reduced CDK1 Y15 phosphorylation significantly correlated with reduced viability in response to 10 µM RO-3306 treatment. Altogether, these data indicate the crucial role of CDK1 activity downstream of OMD in regulating the viability of patient-derived breast cancer samples.

In conclusion, we combined quantitative proteomics and phosphoproteomics from cancer patients with bioinformatics analysis and functional assays *in vitro* and *in vivo* and showed

that OMD regulates cell migration, cell viability and bone metastatic capabilities through a CDK1-dependent mechanism (Fig. 6).

Discussion

The yet unmet clinical need for novel biomarkers and targeted therapies to prevent and treat breast cancer metastasis is demonstrated by the still very high number of deaths from breast cancer each year of which 90% is caused by metastatic disease (2). Here, we combined quantitative proteomics and phosphoproteomics from breast cancer patient-derived samples and cell models with bioinformatics analysis and functional assays and found that the OMD-CDK1 signalling axis drives breast cancer cell motility and viability *in vitro* and bone metastasis *in vivo.*

Our study suggests that proteomics and phosphoproteomics are ideal to identify novel drivers of metastasis to be used as biomarkers or drug targets in the clinic, as often dysregulated genes or RNA transcripts identified in patient samples poorly correlate with the proteomics changes seen in metastases (5, 33). In the future, multi-omics analysis will allow both identification of more robust biomarkers by integrating information at the DNA, RNA and protein level and validation of which mutations actually translate to signalling changes to be used as actionable therapeutic targets (36, 37). Along this line, our manually curated database provides available information on genes and proteins associated with breast cancer metastasis and identifies several omics and multi-omics studies of primary and/or metastatic breast samples, thus offering a vast resource to discover novel biomarkers and drug targets. Among the limitations of proteomics analysis of large cohort of patient samples are the availability of fresh frozen rather than paraffin-embedded (not yet suitable for phosphoproteomics) matched primary and metastatic samples and of the clinical information associated with them. Our proteomics and phosphoproteomics analysis of fresh frozen primary breast cancer resection samples provides therefore a unique resource as samples were manually annotated to determine the presence or absence of organ-specific

metastases within five years of diagnosis, thus overcoming the need for matched metastasis not commonly available in the clinic or limited to a few surgical settings (38, 39). The analysis of bulk tumours may be limited by inter-patient heterogeneity in cellular content between epithelial and stromal cells. Here, to enable good proteome and phosphoproteome coverage of epithelial cells compared to other cell type we developed a very easy to implement and cost-effective fractionation method compared to previously used super-SILAC boosting and extensive fractionation (5). In the foreseeable future, spatial proteomics based on the integration of laser microdissection, artificial intelligence, single cell selection, and mass spectrometry hold promise to specifically identify proteomic differences between the epithelial tumour cells in their microenvironment starting from very low amounts of material (40).

Our proteomics analysis identified OMD, a monomeric member of the small leucine-rich repeat protein (SLRP) family (22), as significantly upregulated in patients who developed bone metastases compared to those who developed metastases at other metastatic sites or who did not develop metastases. The transcript of OMD was previously identified as enriched in breast cancer bone metastases compared to breast cancer metastases in other organs (7) and in prostate cancer bone metastases (21). These findings suggest that OMD may be a pan-cancer biomarker for bone metastases. However, this idea needs clinical validation using, for example, a large retrospective cohort study such as the AZURE trial (41). OMD regulates important cancer pathways, including Ras, P53, Jun/Fos, MYC, and NFkB signalling (20), but little is known about its role in cancer phenotypes. Although our data exclude a primary role for OMD in the tested functions of fibroblasts and osteoclasts using available cell models, OMD may play a role in promoting bone turnover, which is an essential step in osteosclerotic bone metastases (25). Indeed, OMD interacts with BMP2 and promotes induction of transcription factor SP7 and Runt-related transcription factor 2 (RUNX2), both of which are essential for osteogenesis (42). This idea is supported by our observation of increased osteoblast calcium deposition in response to the highest tested

concentrations of rOMD. OMD is known to reduce apoptosis in osteoblasts (28), thus supporting a role for OMD in promoting new bone formation and cell survival. Indeed, in our patient cohort upregulated OMD expression correlates with upregulation of serine 118 phosphorylation on pro-apoptotic protein BCL2-associated agonist of cell death (BAD). This site prevents BAD interaction with BCL2 Like 1, thus preventing apoptosis (43). As BAD serine 118 phosphorylation has been observed in cellular resistance to platinum chemotherapy (44), OMD and BAD could play a similar role in driving the survival of cancer cells in breast cancer patients who develop bone metastases, an hypothesis that deserves further validation. Another intriguing possibility supported by this study is that OMD drives breast cancer bone metastasis by regulating epithelial cancer signalling. Indeed, phosphoproteomics analysis identified a correlation between elevated OMD expression and increased activation of the kinase CDK1 in both cell models and patient samples (8, 37). Therefore, OMD expression may inform clinicians as to which patients could benefit from CDK1 inhibition, although this idea needs further immunohistochemistry validation in larger cohort of samples. Secreted OMD (20) should engage a cell surface receptor, including the BMP2 receptor complex (42), as BMP2 signalling is associated with bone metastasis (45). In support of this idea, we identified BMP2-induced kinase (BMP2K) downstream of OMD in PAO cells. Crosslinking and cell-surface capture mass spectrometry could identify other candidates and elucidate the signalling pathways downstream of OMD in breast and other cancer cells.

Our study reveals that the OMD-CDK1 axis is a driver of cell viability and motility, consistent with the role of CDK1 not only in cell cycle regulation, but also in actin remodelling, a key process in cell migration (46). We also found increased phosphorylation of vimentin on Serine 56, which regulates cancer cell invasion (47), in patients who developed metastases compared to those who did not. The intriguing role of CDK1 as a driver of cell migration and potential metastasis deserves further investigation in breast and other cancers. Indeed, CDK1 mRNA is upregulated not only in several transcriptomics datasets of breast cancer

samples compared to normal breast tissue samples (48), but also in melanoma (49), thyroid cancer (50) and acute myeloid leukaemia (13). Our data suggest that CDK1 inhibition could serve as a novel therapeutic route to prevent or decrease bone metastasis in breast cancer. However, the CDK1 inhibitor RO-3306 has been used in few studies *in vivo* (51, 52) but not in clinical trials in breast or other cancers.. Future studies should aim at testing other CDK1 inhibitors or CDK1 inhibition in combination with other signalling inhibitors. For instance, among the phosphorylated sites significantly upregulated in patients who developed metastases compared to those who did not, we also found phosphorylated ser 641 on catenin alpha 1 (CTNNA1) which activates beta catenin signalling resulting in tumour cell invasion (53) and phosphorylated Thr185/Tyr187 on MAPK1 which are hyperactive in metastatic triple negative breast cancer (10). Therefore, our data provides the rationale for the targeting of MAPK and beta catenin signalling pathways in combination with or independently of CDK1 inhibition to prevent metastasis.

In conclusion, the identification of the OMD-CDK1 axis from a small-to-medium size cohort of patient-derived samples with complete clinical information suggests that similar studies can be performed in any cancer setting including across multiple cancers to identify novel biomarkers, organotropic metastatic drivers, and therapeutic targets.

Conclusion

Here, osteomodulin (OMD) was found to be significantly upregulated in primary breast cancer biopsies of patients who developed metastases within five years of diagnosis, compared to those who did not, and was particularly enriched in patients who developed bone metastases. Osteomodulin significantly increased cell migration and cell viability as well as bone colonisation of MDA-MB-231 breast cancer cells and of cells derived from breast cancer metastatic effusions. Migration, bone colonisation and cell viability were found to be cyclin dependent kinase- 1 (CDK1)-dependent. This study establishes a role for the

OMD-CDK1 axis in predicting and targeting breast cancer bone metastases that will require further validation in patients.

List of abbreviations

ADIRF – Adipogenesis Regulatory Factor

AWERB – Animal Welfare and Ethical Review Body

BAD – BCL2-Associated Agonist of Cell Death

BOM – Bone-tropic MDA-MB-231 cell line variant with lentiviral expression of mApple

BOO - Bone-tropic MDA-MB-231 cell line variant with lentiviral expression of OMD

CAF – Cancer-Associated Fibroblast

CDK1 – Cyclin-Dependent Kinase 1

CK19 – Cytokeratin 19

CMA1 – Chymase 1

COL11A1 – Collagen Type XI Alpha 1 Chain

COL4A1 – Collagen Type IV Alpha 1 Chain

CTHRC1 – Collagen Triple Helix Repeat Containing 1

DMEM – Dulbecco's Modified Eagle Medium

EIF4B – Eukaryotic Translation Initiation Factor 4B

FFPE – Formalin-Fixed Paraffin-Embedded

GO – Gene Ontology

H&E – Haemotoxylin and Eosin

HER2 – Human Epidermal Growth Factor Receptor 2

HER2+ - Human Epidermal Growth Factor Receptor 2-positive Breast Cancer

HR+ - Hormone Receptor Positive Breast Cancer

KEGG – Kyoto Encyclopedia of Genes and Genomes

MAPK1 – Mitogen-Activated Protein Kinase 1

MXRA5 – Matrix Remodelling Associated 5

OGN - Osteoglycin

OMD – Osteomodulin

PAM - Parental MDA-MB-231 cell line with lentiviral expression of mApple

PAO - Parental MDA-MB-231 cell line with lentiviral expression of OMD

PGRMC1 – Progesterone Receptor Membrane Component 1

RANKL - Receptor Activator of NFκB Ligand

RT-PCR – Reverse Transcription Polymerase Chain Reaction

SLRP – Small Leucine-Rich Repeat Protein

SNCG – Synuclein Gamma

STMN1 – Stathmin 1

SYNM - Synemin

TN – Triple Negative Breast Cancer

TNC – Tenascin C

VIM - Vimentin

Declarations

Ethics approval

Early breast cancer samples were collected from patients undergoing surgical resection of the primary tumour at the Manchester University NHS Foundation Trust through the Manchester Cancer Research Centre Biobank. Fully informed consent from all patients was obtained in accordance with local National Research Ethics Service Guidelines (Study Number 12/ROCL/01). Metastatic fluids (ascites or pleural effusions) drained from advanced breast cancer patients were collected at the Christie and South Manchester Hospitals NHS Foundation Trusts through the Manchester Cancer Research Centre Biobank. Fully informed consent from all patients was obtained in accordance with local National Research Ethics Service guidelines (study numbers: 05/ Q1402/25, 05/Q1403/159, and 12/ROCL/01).

Consent for publication

na

Data Availability Statement

All raw MS data were generated by the authors and deposited to the ProteomeXchange Consortium, via the PRIDE partner repository with the dataset identifier PXD041719 (Username: reviewer_pxd041719@ebi.ac.uk; Password: 4PS3MTqM); PXD041720 (Username: reviewer_pxd041720@ebi.ac.uk; Password: Tr6QtMFt); PXD042764 (Username: reviewer_pxd042764@ebi.ac.uk; Password: rsDlM5NX).

The R scripts related to this publication are freely accessible at https://github.com/Joseph-Parsons/OMD/.

Competing and non-financial competing interests

The authors declare no potential conflicts of interest. All authors give consent for publication.

Funding

JP: CR-UK Non-Clinical Training Award A27445; PF, DB, JF, MPS, CF: Wellcome Trust (107636/ Z/15/Z and 107636/Z/15/A), the Biotechnology and Biological Sciences Research Council (BB/X001970/1) and Medical Research Council (MR/T016043/1), the NNF Young Investigator Award (call 2022, NNF22OC0070845). JW: Medical Research Council (MR/T016043/1). SC: Engineering and Physical Sciences Research Council. HH, KS: Breast Cancer Now. KT: Stanley Center for Psychiatric Research at Broad Institute. TK, NA: NIHR Manchester Biomedical Research Centre. CB: Cancer Research UK Manchester Institute Histology Core Facility. COB: National Institute for Health Research. RBC: Cancer Research UK, National Institute for Health Research, UK Research and Innovation, Breast Cancer Now. For the purpose of open access, the author has applied a CC BY public copyright licence to any Author Accepted Manuscript version arising from this submission.

Author contributions

HH and SC performed the analysis of CDK1 inhibition *in vivo* experiment. TK helped preparing metastatic effusion samples for mass spectrometry analysis. PF prepared all samples for mass spectrometry-based proteomic analysis. KS helped with in vivo experiments and Alamar blue viability analysis. DB helped with osteoblast alkaline phosphatase activity assay, osteoblast Alizarin red staining and osteoclast pore forming assays and their analysis. JF helped cloning and supervised cell work. JW and KT provided code for the analysis of mass spectrometry data. CB optimised the immunohistochemistry analysis. N analysed epithelial content of H&E slides from patient resection sample sections. MPS designed the CDK1 inhibitory experiments. COB devised the project and collated information on patient samples for mass spectrometry-based analysis. RBC devised the project and designed in vivo experiments. CF devised the project designed mass spectrometry and in vitro experiments and obtained funding for the project. JP performed and analysed all the other experiments. All authors wrote and reviewed the manuscript before submission.

Acknowledgments

We thank the CRUK Manchester Institute Histology and Visualisation, Imaging and Analysis facilities for their support with immunohistochemical optimisation and visualisation, the University of Manchester Bio-MS, Genome Editing, and Imaging facilities for their continuing support throughout the project. We thank Dr Hurlstone, University of Manchester, Prof Brown and Prof Ottewell, Sheffield, for providing invaluable reagents and protocols.

References

1. Nolan E, Lindeman GJ, Visvader JE. Deciphering breast cancer: from biology to the clinic. Cell. 2023;186(8):1708-28.

2. Riggio AI, Varley KE, Welm AL. The lingering mysteries of metastatic recurrence in breast cancer. British Journal of Cancer. 2021;124(1):13-26.

3. Nolan E, Kang Y, Malanchi I. Mechanisms of Organ-Specific Metastasis of Breast Cancer. Cold Spring Harb Perspect Med. 2023.

4. Satcher RL, Zhang XH. Evolving cancer-niche interactions and therapeutic targets during bone metastasis. Nat Rev Cancer. 2022;22(2):85-101.

5. Parsons J, Francavilla C. 'Omics Approaches to Explore the Breast Cancer Landscape. Front Cell Dev Biol. 2019;7:395.

6. Paul MR, Pan TC, Pant DK, Shih NN, Chen Y, Harvey KL, et al. Genomic landscape of metastatic breast cancer identifies preferentially dysregulated pathways and targets. J Clin Invest. 2020;130(8):4252-65.

7. Zhang Y, He W, Zhang S. Seeking for Correlative Genes and Signaling Pathways With Bone Metastasis From Breast Cancer by Integrated Analysis. Front Oncol. 2019;9:138.

8. Krug K, Jaehnig EJ, Satpathy S, Blumenberg L, Karpova A, Anurag M, et al. Proteogenomic Landscape of Breast Cancer Tumorigenesis and Targeted Therapy. Cell. 2020;183(5):1436-56.e31.

9. Anurag M, Jaehnig EJ, Krug K, Lei JT, Bergstrom EJ, Kim B-J, et al. Proteogenomic markers of chemotherapy resistance and response in triple negative breast cancer. Cancer Discovery. 2022:CD-22-0200.

10. Zagorac I, Fernandez-Gaitero S, Penning R, Post H, Bueno MJ, Mouron S, et al. In vivo phosphoproteomics reveals kinase activity profiles that predict treatment outcome in triple-negative breast cancer. Nature Communications. 2018;9(1):3501.

11. Satpathy S, Jaehnig EJ, Krug K, Kim B-J, Saltzman AB, Chan DW, et al. Microscaled proteogenomic methods for precision oncology. Nature Communications. 2020;11(1):532.

12. Bos PD, Zhang XH, Nadal C, Shu W, Gomis RR, Nguyen DX, et al. Genes that mediate breast cancer metastasis to the brain. Nature. 2009;459(7249):1005-9.

13. Kojima K, Shimanuki M, Shikami M, Andreeff M, Nakakuma H. Cyclin-dependent kinase 1 inhibitor RO-3306 enhances p53-mediated Bax activation and mitochondrial apoptosis in AML. Cancer Sci. 2009;100(6):1128-36.

14. O'Hare MJ, Bond J, Clarke C, Takeuchi Y, Atherton AJ, Berry C, et al. Conditional immortalization of freshly isolated human mammary fibroblasts and endothelial cells. Proc Natl Acad Sci U S A. 2001;98(2):646-51.

15. Lampiasi N, Russo R, Kireev I, Strelkova O, Zhironkina O, Zito F. Osteoclasts Differentiation from Murine RAW 264.7 Cells Stimulated by RANKL: Timing and Behavior. Biology (Basel). 2021;10(2).

16. Collin-Osdoby P, Osdoby P. RANKL-Mediated Osteoclast Formation from Murine RAW 264.7 cells. In: Helfrich MH, Ralston SH, editors. Bone Research Protocols. Totowa, NJ: Humana Press; 2012. p. 187-202.

17. Harris SA, Enger RJ, Riggs LB, Spelsberg TC. Development and characterization of a conditionally immortalized human fetal osteoblastic cell line. Journal of Bone and Mineral Research. 1995;10(2):178-86.

18. Watson J, Ferguson HR, Brady RM, Ferguson J, Fullwood P, Mo H, et al. Spatially resolved phosphoproteomics reveals fibroblast growth factor receptor recycling-driven regulation of autophagy and survival. Nat Commun. 2022;13(1):6589.

19. Song K, Yu Z, Zu X, Li G, Hu Z, Xue Y. Collagen Remodeling along Cancer Progression Providing a Novel Opportunity for Cancer Diagnosis and Treatment. Int J Mol Sci. 2022;23(18).

20. Papadaki V, Asada K, Watson JK, Tamura T, Leung A, Hopkins J, et al. Two Secreted Proteoglycans, Activators of Urothelial Cell-Cell Adhesion, Negatively Contribute to Bladder Cancer Initiation and Progression. Cancers (Basel). 2020;12(11).

21. Roudier MP, Winters BR, Coleman I, Lam HM, Zhang X, Coleman R, et al. Characterizing the molecular features of ERG-positive tumors in primary and castration resistant prostate cancer. Prostate. 2016;76(9):810-22.

22. Tashima T, Nagatoishi S, Caaveiro JMM, Nakakido M, Sagara H, Kusano-Arai O, et al. Molecular basis for governing the morphology of type-I collagen fibrils by Osteomodulin. Commun Biol. 2018;1:33.

23. Belhabib I, Zaghdoudi S, Lac C, Bousquet C, Jean C. Extracellular Matrices and Cancer-Associated Fibroblasts: Targets for Cancer Diagnosis and Therapy? Cancers (Basel). 2021;13(14).

24. Pincha N, Saha D, Bhatt T, Zirmire RK, Jamora C. Activation of Fibroblast Contractility via Cell-Cell Interactions and Soluble Signals. Bio Protoc. 2018;8(18):e3021.

25. Macedo F, Ladeira K, Pinho F, Saraiva N, Bonito N, Pinto L, et al. Bone Metastases: An Overview. Oncol Rev. 2017;11(1):321.

26. Rosenberg N, Rosenberg O, Soudry M. Osteoblasts in bone physiology-mini review. Rambam Maimonides Med J. 2012;3(2):e0013.

27. Johnson KA, Hessle L, Vaingankar S, Wennberg C, Mauro S, Narisawa S, et al. Osteoblast tissue-nonspecific alkaline phosphatase antagonizes and regulates PC-1. Am J Physiol Regul Integr Comp Physiol. 2000;279(4):R1365-77.

28. Hamaya E, Fujisawa T, Tamura M. Osteoadherin serves roles in the regulation of apoptosis and growth in MC3T3-E1 osteoblast cells. Int J Mol Med. 2019;44(6):2336-44.

29. Vang Mouritzen M, Jenssen H. Optimized Scratch Assay for In Vitro Testing of Cell Migration with an Automated Optical Camera. J Vis Exp. 2018(138).

30. Hornbeck PV, Kornhauser JM, Tkachev S, Zhang B, Skrzypek E, Murray B, et al. PhosphoSitePlus: a comprehensive resource for investigating the structure and function of

experimentally determined post-translational modifications in man and mouse. Nucleic Acids Res. 2012;40(Database issue):D261-70.

31. Belguise K, Milord S, Galtier F, Moquet-Torcy G, Piechaczyk M, Chalbos D. The PKCθ pathway participates in the aberrant accumulation of Fra-1 protein in invasive ER-negative breast cancer cells. Oncogene. 2012;31(47):4889-97.

32. Potapova TA, Daum JR, Byrd KS, Gorbsky GJ. Fine tuning the cell cycle: activation of the Cdk1 inhibitory phosphorylation pathway during mitotic exit. Mol Biol Cell. 2009;20(6):1737-48.

33. Mertins P, Mani DR, Ruggles KV, Gillette MA, Clauser KR, Wang P, et al. Proteogenomics connects somatic mutations to signalling in breast cancer. Nature. 2016;534(7605):55-62.

34. Vassilev LT, Tovar C, Chen S, Knezevic D, Zhao X, Sun H, et al. Selective small-molecule inhibitor reveals critical mitotic functions of human CDK1. Proc Natl Acad Sci U S A. 2006;103(28):10660-5.

35. Rampersad SN. Multiple applications of Alamar Blue as an indicator of metabolic function and cellular health in cell viability bioassays. Sensors (Basel). 2012;12(9):12347-60.

36. Mo H, Breitling R, Francavilla C, Schwartz J-M. Data integration and mechanistic modelling for breast cancer biology: Current state and future directions. Current Opinion in Endocrine and Metabolic Research. 2022;24:100350.

37. Mertins P, Mani DR, Ruggles KV, Gillette MA, Clauser KR, Wang P, et al. Proteogenomics connects somatic mutations to signalling in breast cancer. Nature. 2016;534(7605):55-62.

38. Watase C, Shiino S, Shimoi T, Noguchi E, Kaneda T, Yamamoto Y, et al. Breast Cancer Brain Metastasis-Overview of Disease State, Treatment Options and Future Perspectives. Cancers (Basel). 2021;13(5).

39. Kycler WL, P. Surgical approach to pulmonary metastases from breast cancer. The Breast Journal. 2011;18(1):52-7.

40. Mund A, Coscia F, Kriston A, Hollandi R, Kovács F, Brunner A-D, et al. Deep Visual Proteomics defines single-cell identity and heterogeneity. Nature Biotechnology. 2022;40(8):1231-40.

41. Garcia-Recio S, Hinoue T, Wheeler GL, Kelly BJ, Garrido-Castro AC, Pascual T, et al. Multiomics in primary and metastatic breast tumors from the AURORA US network finds microenvironment and epigenetic drivers of metastasis. Nat Cancer. 2023;4(1):128-47.

42. Lin W, Zhu X, Gao L, Mao M, Gao D, Huang Z. Osteomodulin positively regulates osteogenesis through interaction with BMP2. Cell Death Dis. 2021;12(2):147.

43. Tan Y, Demeter MR, Ruan H, Comb MJ. BAD Ser-155 Phosphorylation Regulates BAD/Bcl-XL Interaction and Cell Survival *. Journal of Biological Chemistry. 2000;275(33):25865-9.

44. Marchion DC CH, Xiong Y, Chen N, Bicaku E, Fulp WJ, Bansal N, Chon HS, Stickles XB, Kamath SG, Hakam A, Li L, Su D, Moreno C, Judson PL, Berchuk A, Wenham RM, Apte SM, Gonzalez-Bosquet J, Bloom GC, Eschrich SA, Sebti S, Chen DT, Lancaster JM. BAD phosphorylation determines ovarian cancer chemosensitivity and patient survival. Clinical Cancer Research. 2011;17(19).

45. Katsuno Y, Hanyu A, Kanda H, Ishikawa Y, Akiyama F, Iwase T, et al. Bone morphogenetic protein signaling enhances invasion and bone metastasis of breast cancer cells through Smad pathway. Oncogene. 2008;27(49):6322-33.

46. Jones MC, Askari JA, Humphries JD, Humphries MJ. Cell adhesion is regulated by CDK1 during the cell cycle. Journal of Cell Biology. 2018;217(9):3203-18.

47. Ratnayake WS, Apostolatos CA, Breedy S, Dennison CL, Hill R, Acevedo-Duncan M. Atypical PKCs activate Vimentin to facilitate prostate cancer cell motility and invasion. Cell Adh Migr. 2021;15(1):37-57.

48. Li M, He F, Zhang Z, Xiang Z, Hu D. CDK1 serves as a potential prognostic biomarker and target for lung cancer. J Int Med Res. 2020;48(2):300060519897508.

49. Ravindran Menon D, Luo Y, Arcaroli JJ, Liu S, KrishnanKutty LN, Osborne DG, et al. CDK1 Interacts with Sox2 and Promotes Tumor Initiation in Human Melanoma. Cancer Res. 2018;78(23):6561-74.

50. Zheng HP, Huang ZG, He RQ, Lu HP, Dang YW, Lin P, et al. Integrated assessment of CDK1 upregulation in thyroid cancer. Am J Transl Res. 2019;11(12):7233-54.

51. Wu CX, Wang XQ, Chok SH, Man K, Tsang SHY, Chan ACY, et al. Blocking CDK1/PDK1/β-Catenin signaling by CDK1 inhibitor RO3306 increased the efficacy of sorafenib treatment by targeting cancer stem cells in a preclinical model of hepatocellular carcinoma. Theranostics. 2018;8(14):3737-50.

52. Paraghamian SE, Huang Y, Hawkins GM, Fan Y, Yin Y, Zhang X, et al. The Cdk1 inhibitor RO3306 has anti-tumorigenic effects in high-grade serous ovarian cancer. Gynecologic Oncology. 2020;159:88-9.

53. Ji H, Wang J, Nika H, Hawke D, Keezer S, Ge Q, et al. EGF-induced ERK activation promotes CK2-mediated disassociation of alpha-Catenin from beta-Catenin and transactivation of beta-Catenin. Mol Cell. 2009;36(4):547-59.

Figure legends

Fig. 1. Proteomics analysis identifies enrichment of OMD in samples from patients who developed bone metastases **A,** Workflow of the proteomics and phosphoproteomics analysis of patient-derived samples. The characteristics of samples and the numbers of proteins and phosphorylated sites identified are indicated. Tissue and mouse images were downloaded from SmartServier Medical Art. **B, C,** Volcano plots showing differentially expressed proteins (B) or phosphorylated sites (C) based on Limma p value <0.05, Log2 Fold change >1.5 between metastatic and non-metastatic samples. Proteins or sites upregulated in patients who developed metastases are in orange while proteins and sites downregulated in patients who developed metastases are in blue. Proteins and phosphorylated sites previously associated with breast cancer metastasis regulation are labelled. **D,** KEGG and GO terms enrichment analysis of differentially regulated proteins and phosphorylated sites between

metastatic and non-metastatic samples from B and C. Adjusted p values are generated using Fisher's exact test with Benjamini-Hochberg correction. **E**, Osteomodulin (OMD) log2 normalised protein intensity in non-metastatic patients, metastatic patients, patients who developed bone metastases or patients who developed metastases at any other sites not including bone. Data represent mean +/- SEM of 15 non-metastatic samples compared to 20 metastatic samples, and 12 bone-metastatic samples compared to 8 non-bone metastatic samples (Limma p values ** <0.01, *** <0.001, **** <0.0001) and are rvisualised in the same graph. **F,** OMD mRNA levels in bone metastasis and in metastases to other organs from the GEO datasets (https://www.ncbi.nlm.nih.gov/pmc/articles/PMC6424882/). Data (37 bone metastatic patient samples, 148 other metastatic site patient samples) are represented as mean (Limma p values with Benjamini-Hochberg False Discovery Rate Correction < 0.0001****.

Fig. 2. OMD does not affect the responses of fibroblast, osteoblast, and osteoclast cell lines. **A, B,** Immunoblotting analysis with the indicated antibodies of total lysates from MDA-MB-231 cells stably transfected with mApple (PAM) or an OMD-T2A-mApple construct (PAO) and grown in complete or starved medium (A) and of conditioned medium from the same cells (B) N=3 independent biological replicates. **C, D, E,** Collagen contractility assay of HMFU19 immortalised normal fibroblasts (C), 544R immortalised cancer-associated fibroblasts (D) and HFOB 1.19 osteoblasts (E) treated with conditioned medium (CM) from either PAM or PAO and the indicated concentrations of rOMD where collagen plug shrinkage to a % area of its original size over 72 hours represents collagen remodelling compared to time zero. **F, G,** Alkaline phosphatase activity (F) and alizarin red staining (G) of HFOB 1.19 osteoblasts grown at 34°C (undifferentiated) or 39.5^{o}C (differentiated) followed by treatment (or not) with conditioned media or rOMD. **H, I,** Bone resorption assay assessing pit formation (H) and size of pits per well/bone disc (I) of RAW 264.7 monocyte cells differentiated or not to osteoclasts with RANKL and treated or not with conditioned media or rOMD. (C-I) Data is presented as mean +/- SEM of N = 3 independent biological replicates. Experiments with

CM were performed independently of rOMD experiments and were thus not directly compared. p = <0.05 *, <0.01 **, <0.001 ***, <0.0001 **** rOMD (One Way ANOVA with Dunnett's Multiple Comparison Test, compared to untreated control

Fig. 3. OMD regulates cell migration *in vitro* and colonization of the bone *in vivo.* **A, C,** Cell migration of PAM (grey), PAO (red), PAM treated with 10, 100 or 1000 ng/ml of rOMD (A) and of BOM (green) and BOO (blue) (C) assessed by wound density (percentage of the wound filled with cells 48 h post-scratch compared to time zero). Data represents the mean +/- SEM of N = 3 independent biological replicates, each including at least 3 technical triplicates. *p* =< 0.05*, < 0.01**, < 0.001***, < 0.0001**** (One Way ANOVA with Dunnett's Multiple Comparison Test, compared to untreated control. **B, D,** Representative images from A and C, respectively. The yellow lines indicate wound density at 48h. Scale bar = 1mm. **E,** Number of metastatic lung lesions of over 100µm in diameter (in at least 1 dimension) following intracardiac injection of 100,000 PAM, PAO, or BOM cells in N=4 athymic nude mice per condition. **F,** Number of cytokeratin 19-positive human cells identified in cytospun bone flushes following intracardiac injection of 100,000 PAM, PAO, or BOM cells in N=4 athymic nude mice per condition. *p* =< 0.05*, < 0.01**, < 0.001***, < 0.0001**** (Mean +/- SEM, Student's *t*-test, each compared to PAM). **G,** Representative images from F where red arrows indicate CK19-positive areas. Scale bar=1mm.

Fig. 4: Phosphoproteomics identifies the OMD-CDK1 axis in breast cancer cells and patient-derived samples. **A,** Volcano plot showing differentially regulated phosphorylated sites in PAO cells compared to PAM cells based on Limma p value <0.05, Log2 Fold Change >1. Orange, upregulated in PAO; blue, downregulated in PAO; black text, downregulated sites in PAO compared to PAM and in BOO compared to BOM; red text, sites with metastasis-associated functions according to Phosphosite plus. **B, C** Immunoblotting analysis with indicated antibodies of PAM, PAO, BOM and BOO cell lysates (B) followed by quantification by densitometry and normalisation to vinculin (C). Data is presented as the ratio between the intensity of CDK1 phosphorylated on Y15 and the intensity of the loading control. Values

were calculated using Image J and are presented relative to PAM band intensity. N = 3 independent biological replicates *p* =< 0.05*, < 0.01**, < 0.001***, < 0.0001**** (Student's *t*-test). **D, E,** Expression of OMD and of phosphorylated CDK1 on T14, Y15, or Y19 from two independent proteomics and phosphoproteomics datasets (8, 33). Data is presented as mean +/- SEM of Log2 iTRAQ ratios (N=83) and Log TMT ratios (N=122), respectively, and compared to an internal standard. *p* =< 0.05*, < 0.01**, < 0.001***, < 0.0001**** (Student's *t*-test).

Fig. 5. CDK1 regulates cell migration and viability *in vitro* and colonization of the bone *in vivo*. **A, B,** Cell migration of PAM and PAO cells treated either with DMSO and 10μM RO-3306 (CDK1i) (A) and of PAO cells treated either with DMSO, 10μM RO-3306, or 10μM Palbociclib (CDK4,6i) (B) assessed by wound closure over 48hrs and measured by wound density. Data represent the percentage of the wound filled with cells 48 hours post-scratch. N = 3 biologically independent replicates. p =< 0.05*, < 0.01**, < 0.001***, < 0.0001**** (One Way ANOVA with Dunnett's Multiple Comparison Test, compared to untreated control. **C**, **F,** Relative viability of PAM and PAO cells (C) and of cells from 5 metastatic pleural effusion (F) measured by cell fluorescence at 590nm upon reduction of alamar blue stain during incubation with non-adherent cells for 4 hours. Data is presented as mean +/- SEM of N >=3 independent biological replicates. P =< 0.05*, < 0.01**, < 0.001***, < 0.0001**** (Student's t-test). **D,** Number of cytokeratin 19-positive human cells identified in cytospun bone flushes following intracardiac injection of 100,000 PAO cells and treatment with CDK1 inhibitor 4mg/kg RO-3306 or vehicle control 3 times per week for 25 days in N=4 athymic nude mice per condition. p =< 0.05*, < 0.01**, < 0.001***, < 0.0001**** (Mean +/- SEM, Student's t-test, each compared to PAM**). E,** Representative images from C where red arrows indicate CK19-positive areas. Scale bar=1mm**. G,** Correlation between CDK1 Y15 normalised over CDK1 total protein normalised intensity and viability in response to CDK1 inhibition with 10μM RO-3306. Data is presented as mean response to viability, N=4 independent biological

replicates. P =< 0.05*, < 0.01**, < 0.001***, < 0.0001**** (One-sided Linear Regression t test).

Fig. 6. Model of the OMD-CDK1 axis driving breast cancer bone metastasis.

Figure 1

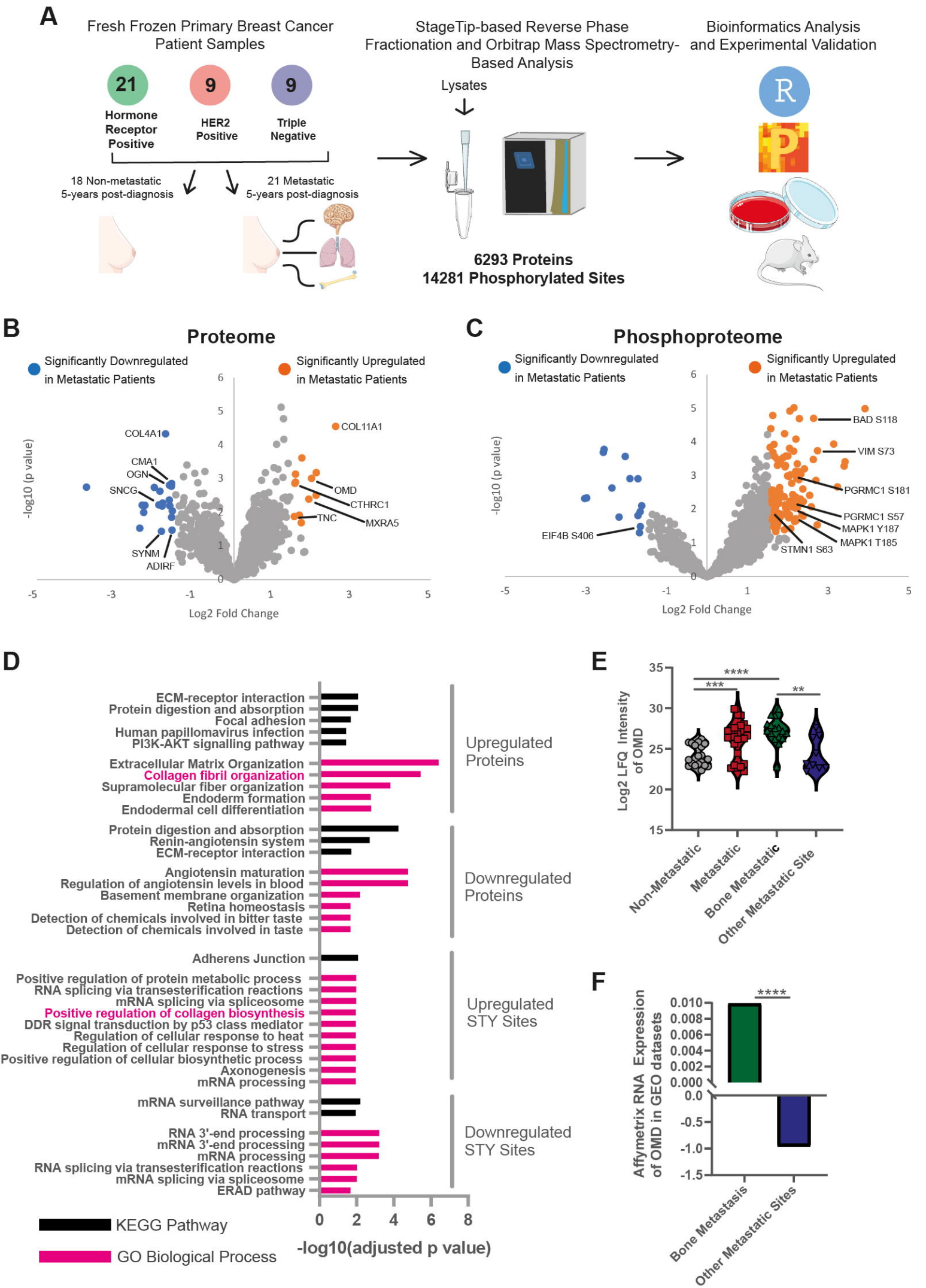
A
Fresh Frozen Primary Breast Cancer Patient Samples
21
Hormone Receptor Positive
9
HER2 Positive
9
Triple Negative
18 Non-metastatic 5-years post-diagnosis
21 Metastatic 5-years post-diagnosis
StageTip-based Reverse Phase Fractionation and Orbitrap Mass Spectrometry-Based Analysis
Lysates
6293 Proteins
14281 Phosphorylated Sites
Bioinformatics Analysis and Experimental Validation
R
B
Proteome
Significantly Downregulated in Metastatic Patients
Significantly Upregulated in Metastatic Patients
COL4A1
CMA1
OGN
SNCG
SYNM
ADIRF
COL11A1
OMD
CTHRC1
TNC
MXRA5
-log10 (p value)
Log2 Fold Change
C
Phosphoproteome
Significantly Downregulated in Metastatic Patients
Significantly Upregulated in Metastatic Patients
BAD S118
VIM S73
PGRMC1 S181
PGRMC1 S57
MAPK1 Y187
MAPK1 T185
STMN1 S63
EIF4B S406
-log10 (p value)
Log2 Fold Change
D
ECM-receptor interaction
Protein digestion and absorption
Focal adhesion
Human papillomavirus infection
PI3K-AKT signalling pathway
Extracellular Matrix Organization
Collagen fibril organization
Supramolecular fiber organization
Endoderm formation
Endodermal cell differentiation
Protein digestion and absorption
Renin-angiotensin system
ECM-receptor interaction
Angiotensin maturation
Regulation of angiotensin levels in blood
Basement membrane organization
Retina homeostasis
Detection of chemicals involved in bitter taste
Detection of chemicals involved in taste
Adherens Junction
Positive regulation of protein metabolic process
RNA splicing via transesterification reactions
mRNA splicing via spliceosome
Positive regulation of collagen biosynthesis
DDR signal transduction by p53 class mediator
Regulation of cellular response to heat
Regulation of cellular response to stress
Positive regulation of cellular biosynthetic process
Axonogenesis
mRNA processing
mRNA surveillance pathway
RNA transport
RNA 3'-end processing
mRNA 3'-end processing
mRNA processing
RNA splicing via transesterification reactions
mRNA splicing via spliceosome
ERAD pathway
Upregulated Proteins
Downregulated Proteins
Upregulated STY Sites
Downregulated STY Sites
KEGG Pathway
GO Biological Process
-log10(adjusted p value)
E
Log2 LFQ Intensity of OMD
Non-Metastatic
Metastatic
Bone Metastatic
Other Metastatic Site
F
Affymetrix RNA Expression of OMD in GEO datasets
Bone Metastasis
Other Metastatic Sites

Figure 2

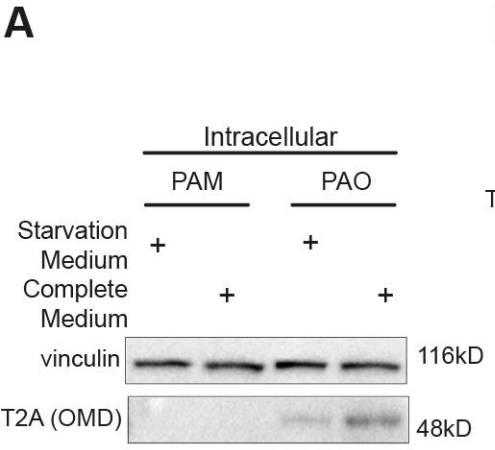
A
Intracellular
PAM
PAO
Starvation Medium
Complete Medium
vinculin
116kD
T2A (OMD)
48kD

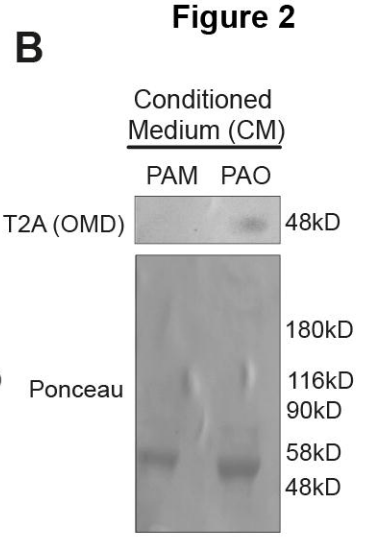
B
Conditioned Medium (CM)
PAM
PAO
T2A (OMD)
48kD
Ponceau
180kD
116kD
90kD
58kD
48kD

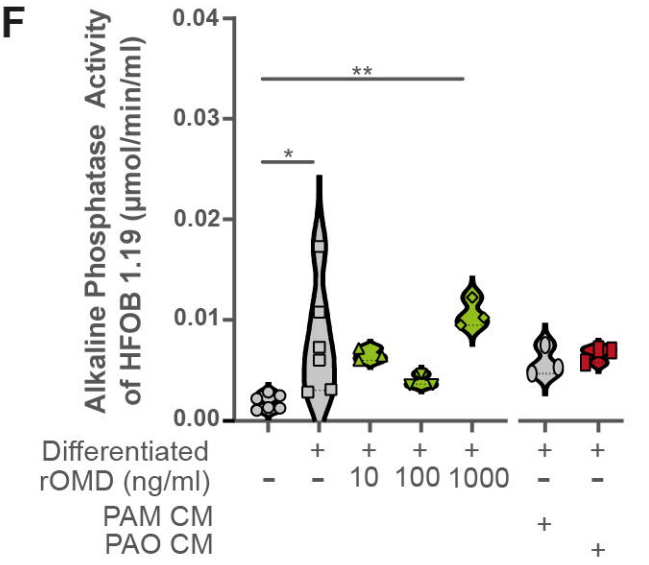
F
Alkaline Phosphatase Activity of HFOB 1.19 (µmol/min/ml)
Differentiated
rOMD (ng/ml)
10
100
1000
PAM CM
PAO CM

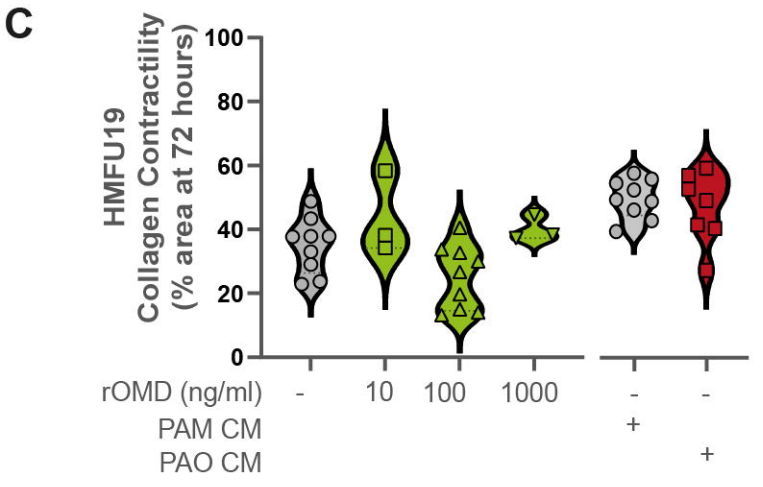
C
HMFU19 Collagen Contractility (% area at 72 hours)
rOMD (ng/ml)
10
100
1000
PAM CM
PAO CM

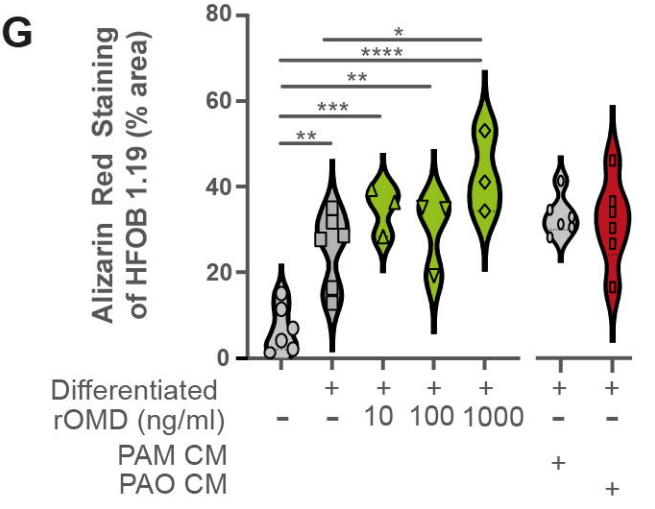
G
Alizarin Red Staining of HFOB 1.19 (% area)
Differentiated
rOMD (ng/ml)
10
100
1000
PAM CM
PAO CM

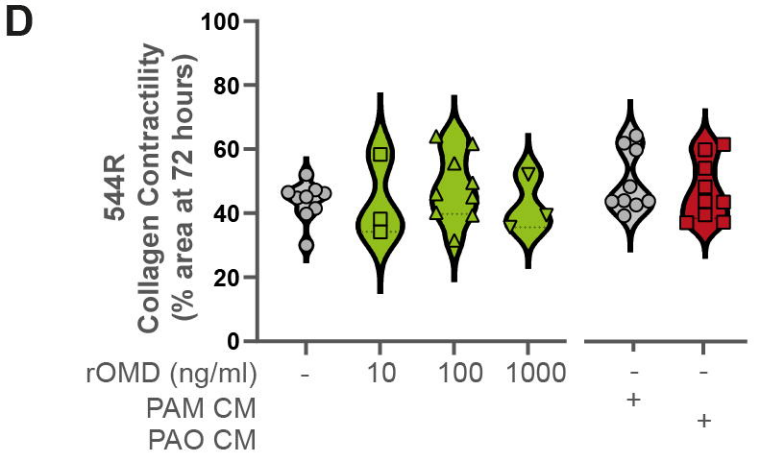
D
544R Collagen Contractility (% area at 72 hours)
rOMD (ng/ml)
10
100
1000
PAM CM
PAO CM

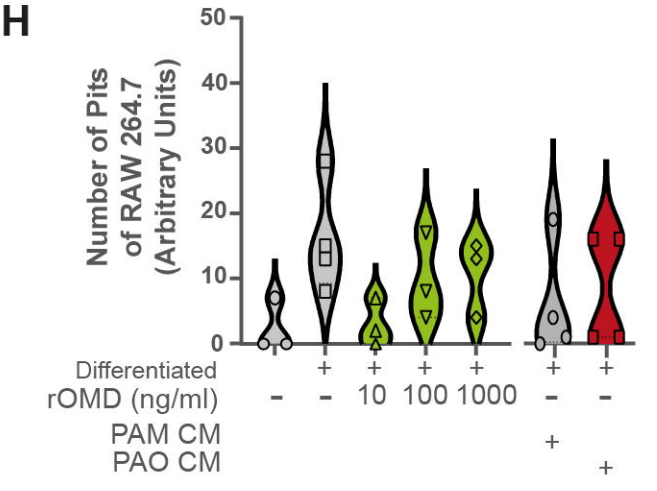
H
Number of Pits of RAW 264.7 (Arbitrary Units)
Differentiated
rOMD (ng/ml)
10
100
1000
PAM CM
PAO CM

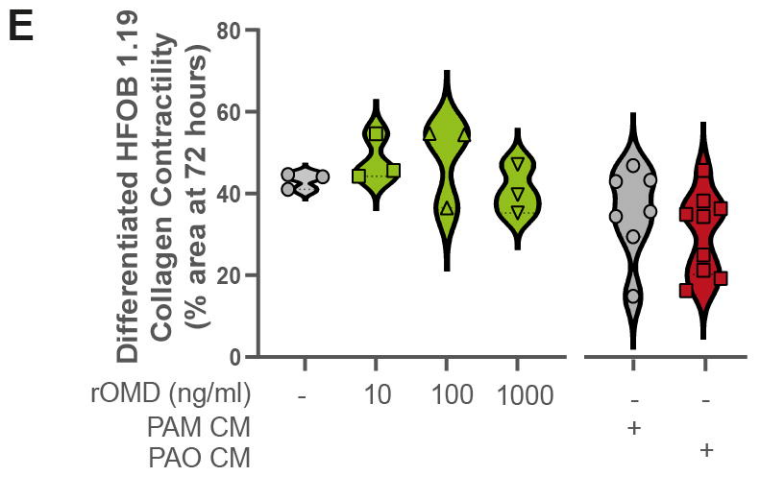
E
Differentiated HFOB 1.19 Collagen Contractility (% area at 72 hours)
rOMD (ng/ml)
10
100
1000
PAM CM
PAO CM

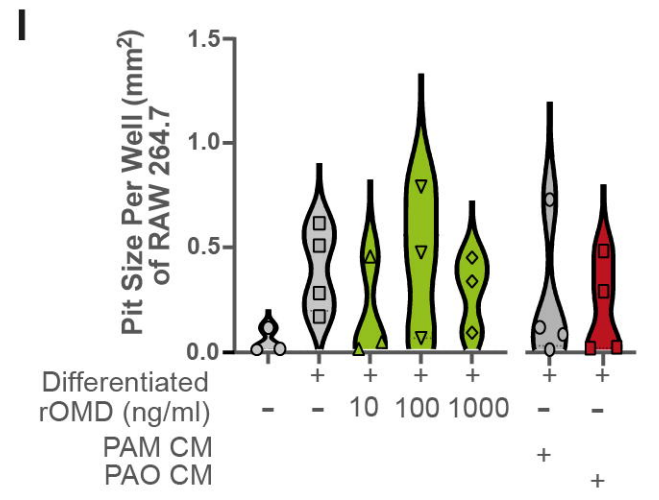
I
Pit Size Per Well (mm²) of RAW 264.7
Differentiated
rOMD (ng/ml)
10
100
1000
PAM CM
PAO CM

Figure 3

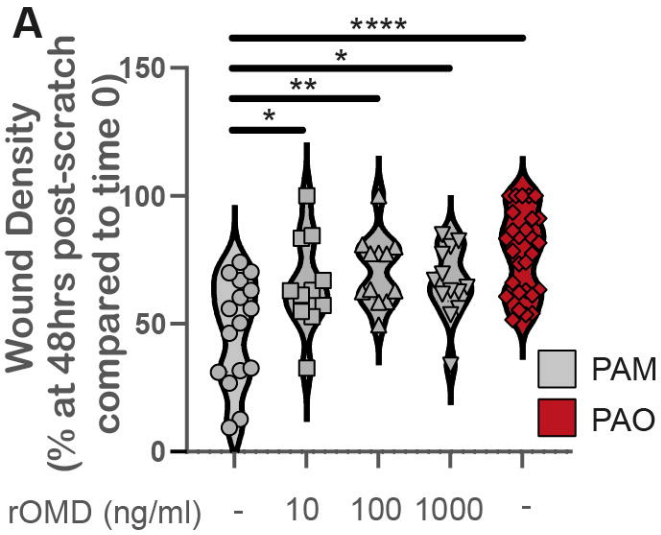
A
Wound Density
(% at 48hrs post-scratch
compared to time 0)
150
100
50
0
****
*
**
*
PAM
PAO
rOMD (ng/ml)
-
10
100
1000
-

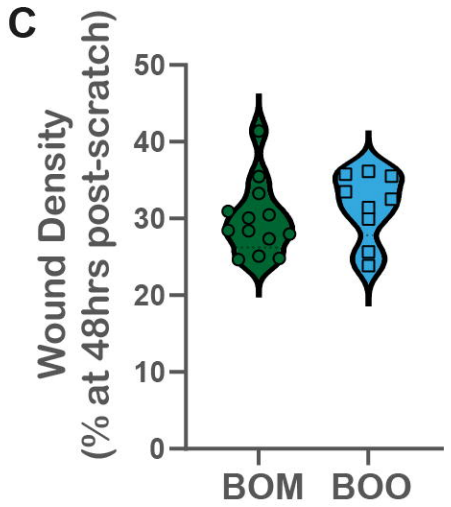
C
Wound Density
(% at 48hrs post-scratch)
50
40
30
20
10
0
BOM
BOO

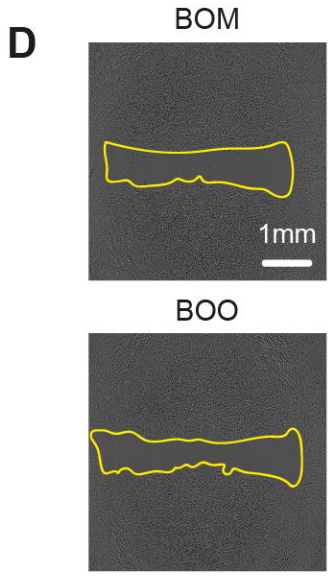
D
BOM
1mm
BOO

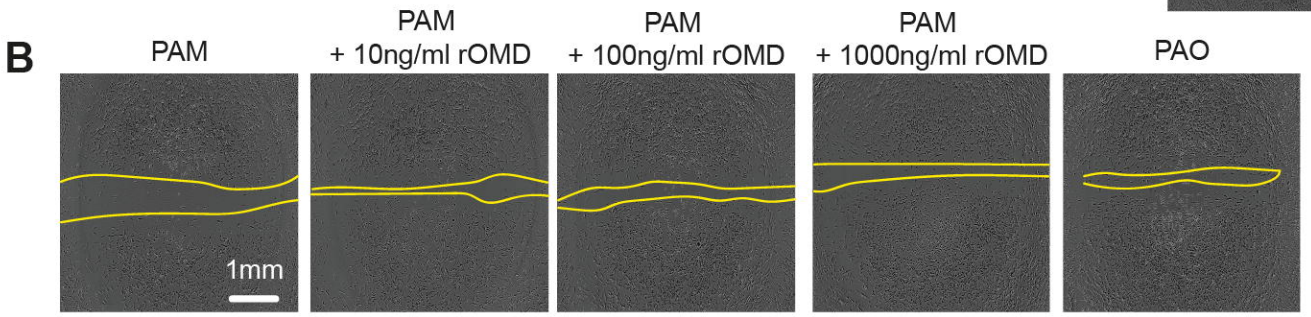
B
PAM
PAM
+ 10ng/ml rOMD
PAM
+ 100ng/ml rOMD
PAM
+ 1000ng/ml rOMD
PAO
1mm

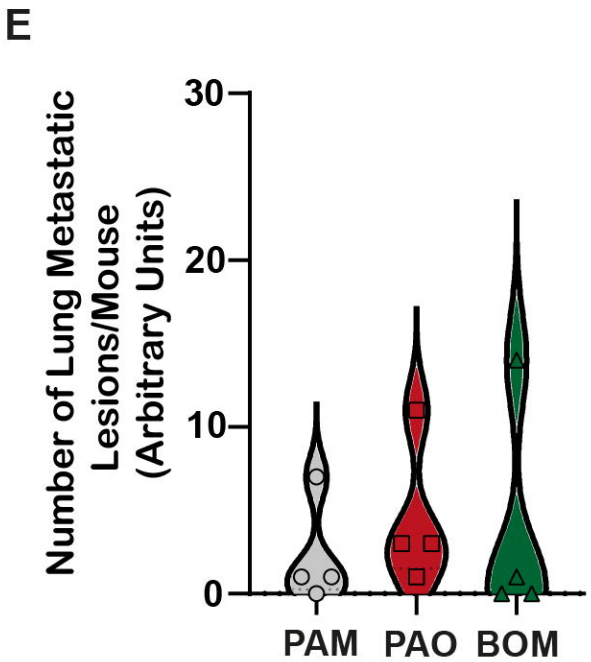
E
Number of Lung Metastatic
Lesions/Mouse
(Arbitrary Units)
30
20
10
0
PAM
PAO
BOM

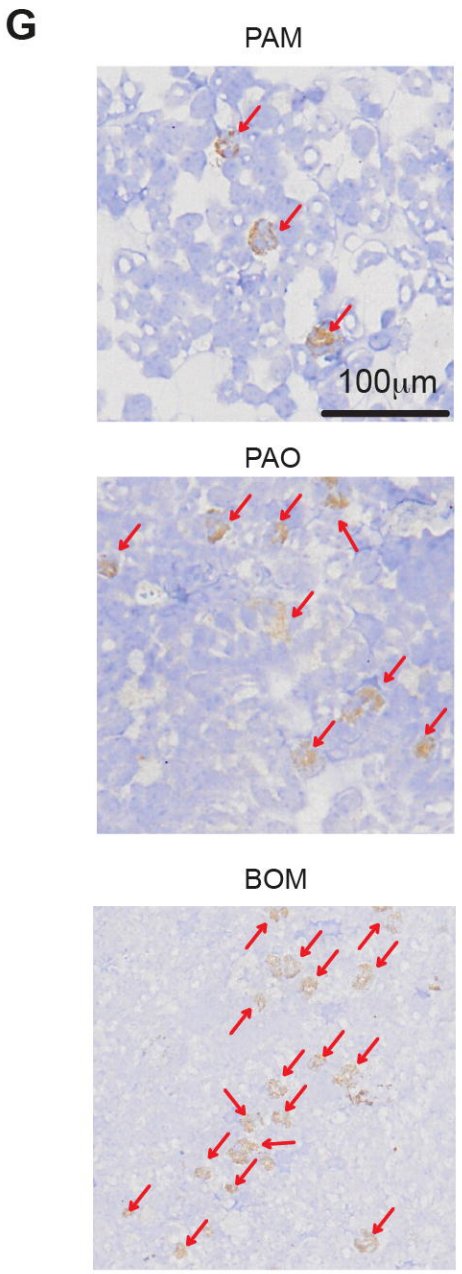
G
PAM
100µm
PAO
BOM

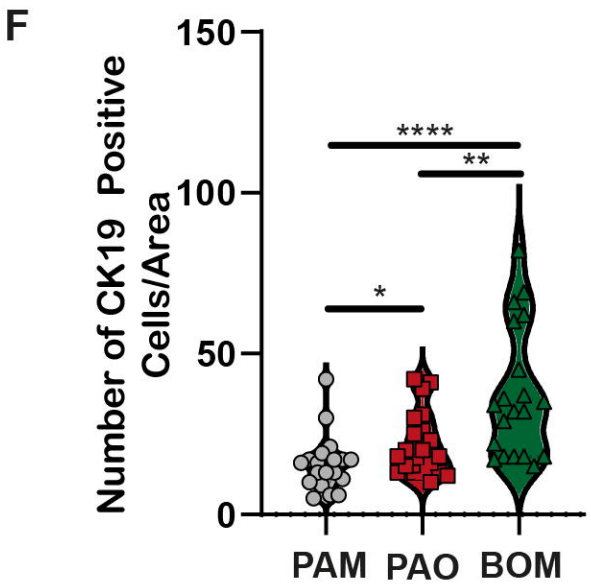
F
Number of CK19 Positive
Cells/Area
150
100
50
0
****
**
*
PAM
PAO
BOM

Figure 4

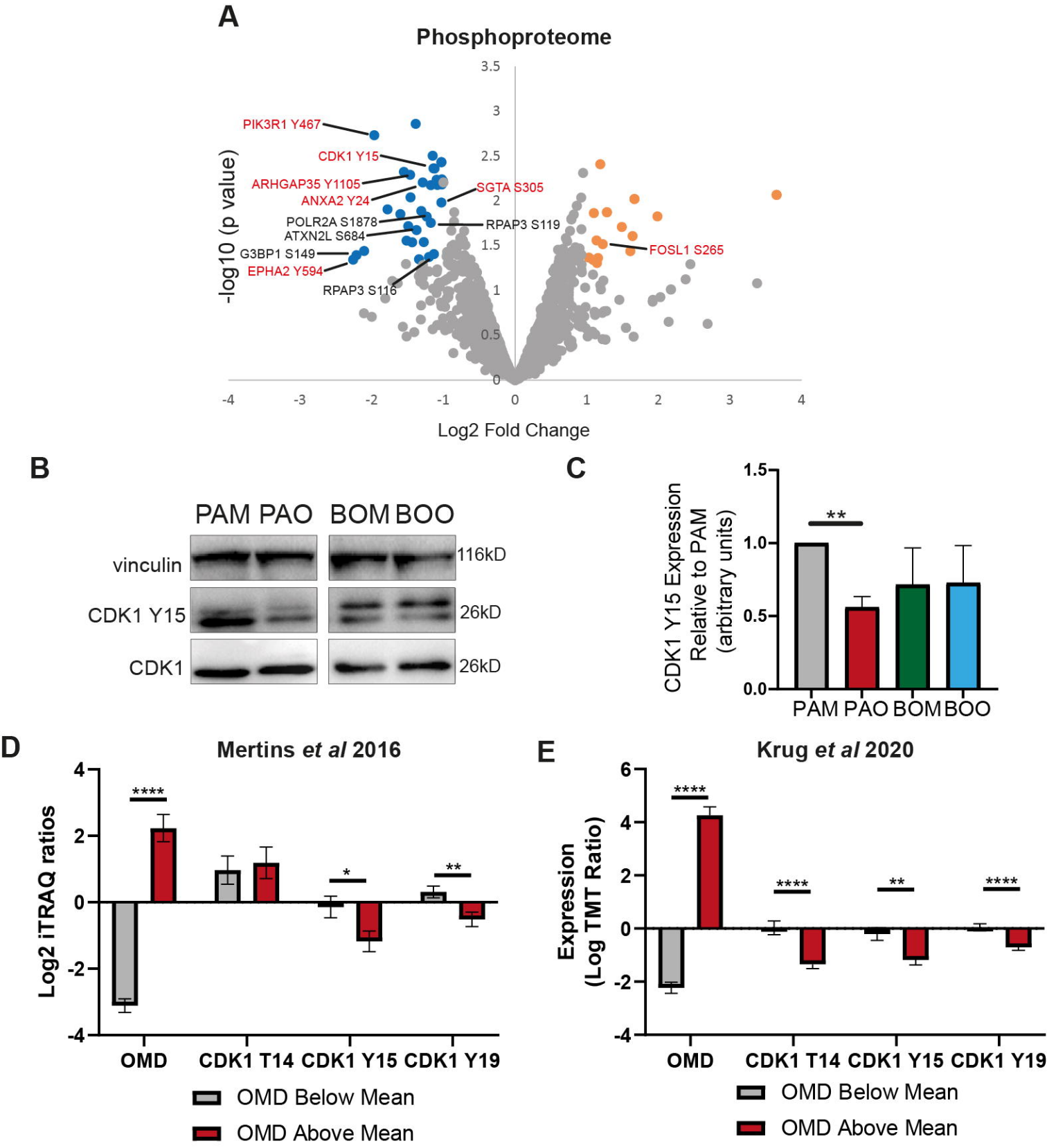
A
Phosphoproteome
-log10 (p value)
Log2 Fold Change
PIK3R1 Y467
CDK1 Y15
ARHGAP35 Y1105
ANXA2 Y24
POLR2A S1878
ATXN2L S684
G3BP1 S149
EPHA2 Y594
RPAP3 S116
SGTA S305
RPAP3 S119
FOSL1 S265
B
PAM PAO BOM BOO
vinculin
CDK1 Y15
CDK1
116kD
26kD
26kD
C
CDK1 Y15 Expression Relative to PAM (arbitrary units)
PAM PAO BOM BOO
D
Mertins et al 2016
Log2 iTRAQ ratios
OMD
CDK1 T14
CDK1 Y15
CDK1 Y19
OMD Below Mean
OMD Above Mean
E
Krug et al 2020
Expression (Log TMT Ratio)
OMD
CDK1 T14
CDK1 Y15
CDK1 Y19
OMD Below Mean
OMD Above Mean

Figure 5

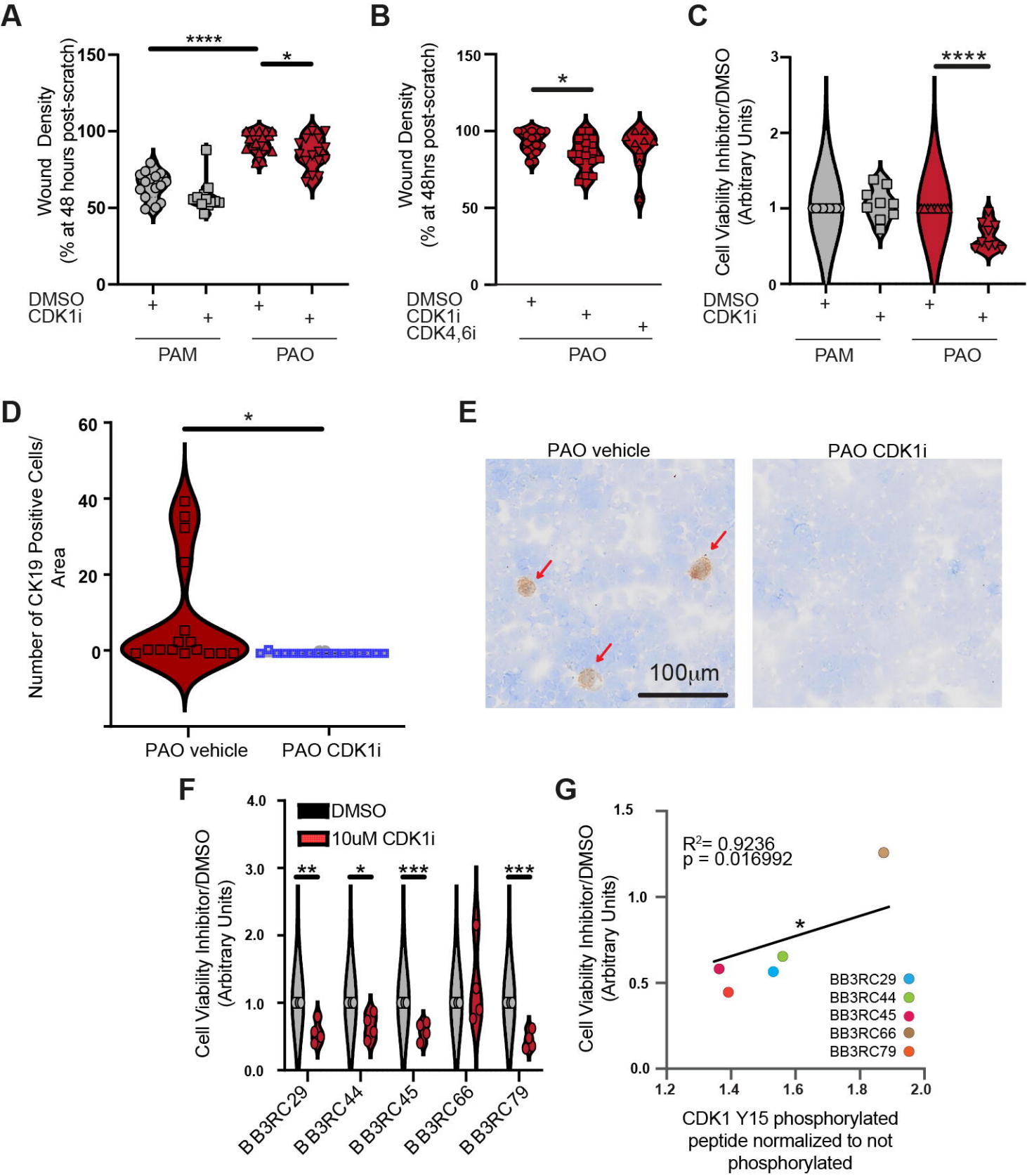
A
Wound Density (% at 48 hours post-scratch)
150
100
50
0
****
*
DMSO
CDK1i
PAM
PAO
B
Wound Density (% at 48hrs post-scratch)
150
100
50
0
*
DMSO
CDK1i
CDK4,6i
PAO
C
Cell Viability Inhibitor/DMSO (Arbitrary Units)
3
2
1
0
****
DMSO
CDK1i
PAM
PAO
D
Number of CK19 Positive Cells/ Area
60
40
20
0
*
PAO vehicle
PAO CDK1i
E
PAO vehicle
PAO CDK1i
100µm
F
Cell Viability Inhibitor/DMSO (Arbitrary Units)
4.0
3.0
2.0
1.0
0.0
DMSO
10uM CDK1i
**
*
***
***
BB3RC29
BB3RC44
BB3RC45
BB3RC66
BB3RC79
G
Cell Viability Inhibitor/DMSO (Arbitrary Units)
1.5
1.0
0.5
0.0
R²= 0.9236
p = 0.016992
*
BB3RC29
BB3RC44
BB3RC45
BB3RC66
BB3RC79
1.2
1.4
1.6
1.8
2.0
CDK1 Y15 phosphorylated peptide normalized to not phosphorylated

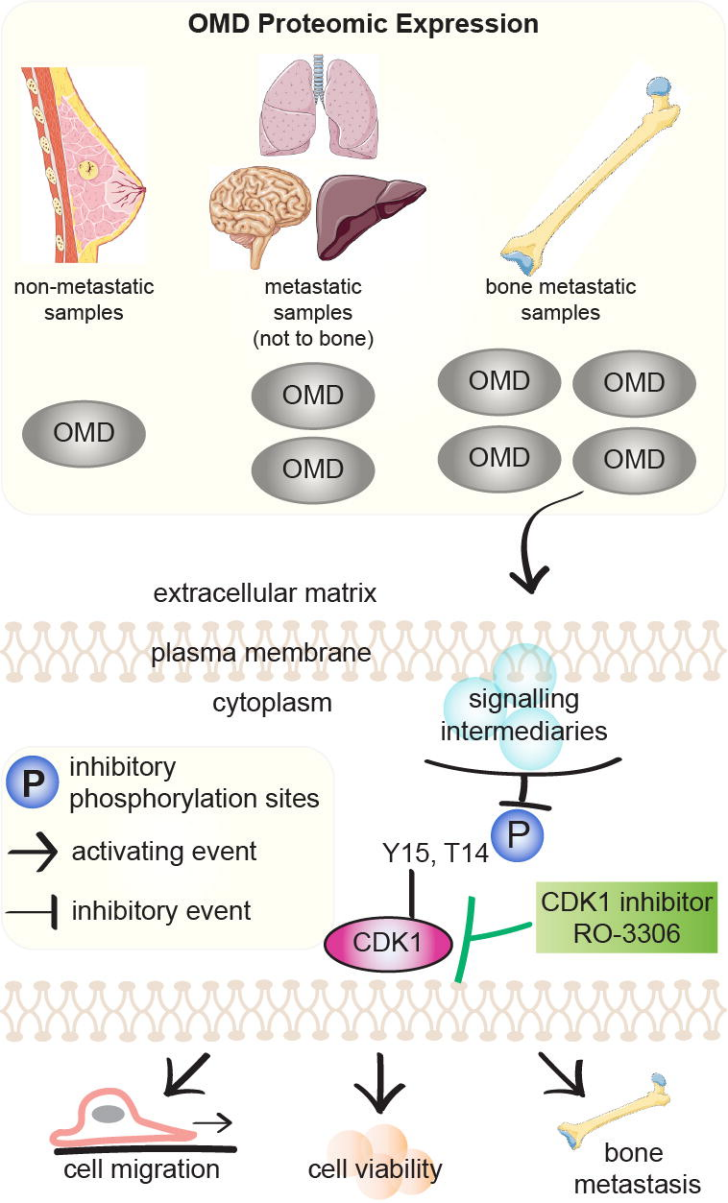
OMD Proteomic Expression
non-metastatic samples
metastatic samples (not to bone)
bone metastatic samples
OMD
OMD
OMD
OMD
OMD
OMD
OMD
extracellular matrix
plasma membrane
cytoplasm
signalling intermediaries
P
inhibitory phosphorylation sites
activating event
inhibitory event
P
Y15, T14
CDK1
CDK1 inhibitor RO-3306
cell migration
cell viability
bone metastasis